ESTUDIO DE LA RETRODISPERSIÓN γ EN CAPAS DE SUELO CON DIFERENTE ESPESOR Y CONTENIDO DE AGUA

JUANSEBASTIAN GÓMEZ MUÑOZ

Trabajo investigativo presentado para optar al título de
Físico

Director
Dr. FERNANDO CRISTANCHO MEJÍA

Universidad Nacional de Colombia
Facultad de Ciencias, Departamento de Física
grupo de física nuclear
Bogotá D.C., Colombia
2012

Study of γ–backscattering in soil layers with different thicknesses and water content

Juansebastian Gómez Muñoz

Advisor
Dr. Fernando Cristancho Mejía

Universidad Nacional de Colombia
Faculty of Sciences, Departament of Physics
nuclear physics group
Bogotá, Colombia
2012

RESUMEN

El tema del presente trabajo es el estudio de la interacción de rayos γ cuando estos son retrodispersados en diferentes tipos de suelo y bajo diferentes condiciones de humedad. La retrodispersión de rayos gamma ha sido utilizada para estudiar las propiedades del suelo o buscar objetos enterrados; estas aplicaciones requieren la comprensión de la interacción de rayos γ con el suelo. Debido a que la sección eficaz de los principales procesos de interacción de la radiación γ con la materia dependen del número atómico de los elementos del blanco, a través del estudio de las intensidades y las energias de los fotones retrodispersados por capas de suelo de diferente espesor, podemos caracterizar la interacción de la radiación con los materiales de la muestra.

El trabajo experimental se realizó utilizando muestras de tierra negra (suelo franco) con diferente espesor y diferente humedad. El montaje experimental consiste en dos detectores de radiación γ conectados en coincidencias temporales y una fuente radioactiva de ^{22}Na. De los espectros de retrodispersión se puede conocer la intensidad relativa de fotones dispersados, una o múltiples veces, como una función del espesor de las capas de suelo y su contenido de agua, y también se encuentra el valor medio de profundidad para el cual es aplicable la técnica. Los resultados para el suelo franco son comparados con los resultados obtenidos previamente para muestras de arena.

ABSTRACT

The subject of this work is the study of the backscattering of γ-rays in different soil types with different water content conditions. Backscattering of γ-rays has been used to study soil properties or to find buried objects. These applications require the understanding of the interaction of γ-rays with soil. Because the cross section of the main processes of interaction of γ radiation with matter depend on the atomic number of the elements of the target, through the study of the intensities and energies of photons backscattered by soil layers of different thicknesses, we can characterize the interaction of radiation with the sample materials.

The experimental work was developed using samples of farming soil with different thicknesses and different water content. The experimental setup consists of two γ detectors connected in fast time coincidences and a radioactive source of ^{22}Na. Spectra of backscattered γ-rays are obtained and an approach to distinguish between single and multiple backscattered photons is presented in wich their relative intensity as a function of layer thickness and water content is analyzed. The results for the farming soil are compared with results obtained previously for sand samples.

A Mercedes y Otto,
por la vida, el apoyo y la paciencia,
por su amor, y por darme la libertad para construir mi camino.

"y loa tú, alma mía, al Señor Creador tuyo, mientras yo fuere: pues de Él y por Él y en Él son cuantas cosas son, las de los sentidos y las del entendimiento, así las que ignoramos por completo como las que sabemos, parte mínima de aquéllas, porque hay más, allende."

Las Armonías del Mundo, Johannes Kepler.

Pero no debes temer que el aprendizaje se convierta en una parte de ti mismo, de modo que te resulte tan natural como respirar. Tienes que expandir tu mente lo suficiente como para que asimile todo cuanto podamos transmitirte.

El Médico, Noah Gordon.

–Adieu, dit le renard. Voici mon secret. Il est très simple: on ne voit bien qu'avec le cœur. L'essentiel est invisible pour les yeux.

Le Petit Prince, Antonie De Saint-Exupéry.

ACKNOWLEDGEMENTS

Learning is a journey, a journey with ups and downs, with opportunities to advance, with obstacles to surpass and time for practice a important thing: to stand up after fall.

I am very grateful with all the people I found in this journey, starting with my advisor, Fernando Cristancho for give me the opportunity to work in the applied nuclear physics laboratory, for each question, their orientation and all the patience he had teaching me. To Liliana Cortés for her time and for all the knowledge she share with me, also her attention to my questions via e-mail. To Zandra Silva for always outstanding, ready to teach and support. Special thanks to partners and friends in gfnun's office, for their time to share academic questions, some personal questions and other issues to have a good time.

Of course, I want to thank to the Professors of Department of Physics for their teaching and advice in every area of physics, especially those who guided me in the adventure that means every historical and basic experiment.

It have not been possible this journey without support of my parents, this work is dedicated to them, neither without the advices of my sisters Juliana and Diana. Very thanks to Eliana because the companionship, love and time are essential to follow my dreams. Thanks to Andrea and David for each time our journey crossed and we share a coffee.

The journey don't finish yet and challenges to come are new roads to walk.

CONTENTS

LIST OF FIGURES

CHAPTER 1

INTRODUCTION

Backscattering of γ-rays has been used to study soil properties or to find buried objects. These applications require an understanding of the interaction of γ-rays with soil [1, 2, 3, 4]. The success of the endeavour of obtaining images with backscattered γ-rays [5, 6] supposes the improvement of our knowledge of the processes taking place when a monoenergetic γ-beam inpinges on a multielemental sample with eventual non uniform mass density [7, 8]. Whereas the Klein-Nishina formula for the angular distribution of the scattered intensity is a powerful tool whenever only Single Scattering (SS) is to be taken into account, the same formula loses its analytical capacity in the already described more complex case because the non-uniformity and the multielemental nature, together with the geometrical effects, e.g. size and shape, combine to produce a highly complex situation very far from any analytical treatment since the main effect becomes that of the Multiple Scattering (MS). In this case a given γ-ray scatters several times, changing randomly direction of propagation and energy at each interaction, before arriving to the imaging device. The γ-radiation that the imaging detector receives then is a complex distribution in energy reflecting the response of the macroscopic sample to the γ-beam. Numerical simulation becomes the only meaningful mathematical approach able to produce useful information. Given the necessary high complexity of the simulation codes, their results must be checked very critically. In order to eliminate part of this complexity, and to be able of obtaining a meaningful description, we choose a convenient experimental setup and perform a corresponding simplified analysis. Because the cross section of the main processes of interaction of γ radiation with matter depend on the atomic number of the elements of the target, through the study of the intensities and energies of photons backscattered by layers of soil of different thicknesses, we can characterize the interaction of radiation with the sample materials.

The concept of Compton camera

The Compton camera is a γ-backscattering imaging device that allows us to obtain images of hidden objects [6, 9], it is of particular interest in this work. The nuclear physics group of the Universidad Nacional de Colombia (gfnun) together with the GSI Helmholtzzentrum für Schwerionenforschung are nowadays working with a prototype of this device. The schematic setup of the instrument is shown in Figure 1.1.

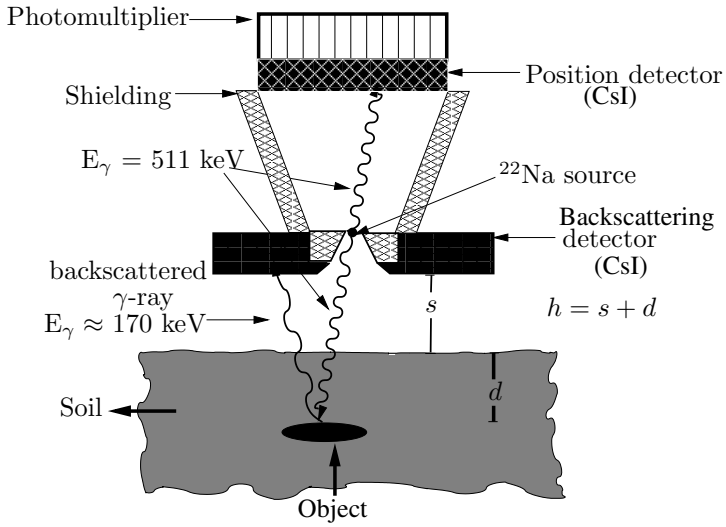

Figure 1.1: Schematic setup of the Compton camera [9].

A ^{22}Na source is placed in the center of a conic lead shielding. In the top of the shielding is placed a position-sensitive detector. A ring-shaped detector is enclosing the source and is used as a backscattering detector. ^{22}Na emits positrons which rapidly annihilate with electrons. The annihilation of each electron-positron pair produces two γ-rays of 511 keV traveling in opposite directions. One of these photons can be detected in the position detector, a CsI crystal coupled to a position-sensitive photomultiplier. The other γ-ray goes into the soil where it can be absorbed or backscattered. If the photon is backscattered it can be detected in the backscattering detector. The device produces an image with the backscattered γ-rays counted in the position detector in coincidence with the other detector [9]. We are supposing that the quality of the obtained image can be improved by taking into account only photons that undergo single scattering in the soil.

The subject of this paper is the study of the interaction of γ-rays with layers of farming soil, varying both its humidity and thicknesses, the purpose is to be able to differentiate the contribution of the SS and MS radiation arriving to a detector. The experimental

setup uses the positron decay of a ^{22}Na source, and two γ detectors (Ge and Plastic scintillator) connected in coincidences. Backscattered spectra are obtained for different humidity values and layer thicknesses and analyzed in order to obtain information about the interaction processes. First, in Chapter 2, a review of the main concepts needed will be made, these concepts include soil physical properties, models of the interaction of radiation with matter and general properties of detection systems. In Chapter 3, the experimental setup, geometrical and electronic, will be described. The Chapter 4 shows the results obtained and the analysis performed on the backscattering spectra. Conclusions and perspectives are summarized in Chapter 5.

CHAPTER 2

THEORETICAL BACKGROUND

The next sections describes the main concepts, include models on the interaction of radiation with matter, general properties of detection systems and soil physical properties.

2.1 Interaction of radiation with matter

The main interactions of γ-rays in matter are: the photoelectric effect, Compton scattering and pair production; this three major types play an important role in radiation measurements [10, 11]. The photoelectric effect involves the absorption of a photon by an atomic electron with the subsequent ejection of the electron from the atom. The energy of the outgoing electron is then

$$E_\gamma = h\nu - \phi$$

where ϕ is the binding energy of the electron. Also, as a result of this process, characteristic X-rays are emitted because of the rearranging of electrons inside the atom. The photoelectric effect cross section, increases at low energies, and has peaks where the K-shell or L-shell energy is approached. Theoretically, the photoelectric effect is difficult to treat rigorously because of the complexity of the Dirac wave functions for the atomic electrons. By assuming that the beam only interacts with electrons in the K-shell and that their energy is not relativistic, it is possible to calculate the photoelectric cross section, σ_{ph}, by using a Born approximation. The functional form of the solution turns out to be

$$\sigma_{\text{ph}} \propto \frac{Z^n}{E_\gamma^{3.5}}$$

where Z is the atomic number of the material and the exponent n varies between 4 and 5. As energy decreases, σ_{ph} increases rapidly, thus low energy beams will be strongly

attenuated by the material and there will be few or no transmission or scattering. We can also see, that $\sigma_{\rm ph}$ increases as the fourth or fifth power of Z therefore, even for high energies, if the absorber material has a high atomic number, $\sigma_{\rm ph}$ will increase and no γ-rays will be transmitted or scattered.

The interaction process of Compton scattering takes place between the incident γ-ray photon and an electron in the absorbing material. The incoming γ-ray is deflected in an angle θ with respect to its original direction. In this process, the photon gives part of its energy to an electron of the material (called recoil electron) and is scattered with a lower energy. Since all scattering angles are possible, the energy of the scattered γ-ray presents a distribution. For the case of interaction with a free electron, the relation between the energy of the scattered photon, E'_γ, and the scattering angle is

$$E'_\gamma = \frac{E_\gamma}{1 + \epsilon\,(1 - \cos\theta)} \tag{2.1}$$

where $\epsilon = E_\gamma / m_e c^2$ is the initial energy of the γ-ray divided by the rest mass-energy of the electron (511 keV). For small scattering angles θ, very little energy is transferred. Some of the original energy is always retained by the incident photon, even in the extreme of $\theta = \pi$. The angular distribution of scattered γ-rays is predicted by the Klein-Nishina formula for the differential scattering cross section $d\sigma/d\Omega$,

$$\frac{d\sigma}{d\Omega} = \frac{r_e^2}{2} \frac{1}{[1 + \epsilon(1 - \cos\theta)]^2} \left(1 + \cos^2\theta + \frac{\epsilon^2 (1 - \cos\theta)^2}{1 + \epsilon(1 - \cos\theta)} \right), \tag{2.2}$$

it gives the differential scattering cross section per solid angle unit. Integration of this formula over $d\Omega$ gives the total probability per electron for Compton scattering, σ_C, to occur. In order to obtain the total Compton cross section per scattering center, it is necessary to multiply this formula by Z. Figure 2.1 shows a polar plot of the Klein-Nishina formula for different energies. We can see from the Figure that there is a strong tendency to forward scattering for all energies. In fact, as energy increases the backscattering probability decreases rapidly. Thus, high energy beams will not be suitable for backscattering applications.

Pair production consists in the interaction of a photon with the nuclear field. If the γ-ray energy exceeds twice the rest-mass energy of an electron (1022 keV), the process of pair production is energetically possible. In the process, the γ-ray disappears and is replaced by an electron-positron pair. The excess energy carried by the photon above 1022 keV goes to kinetic energy of the pair. Since the positron will annihilate with an electron of the medium, two 511 keV γ-rays will also be produced in this process. The cross section for pair production, σ_{pp} is considerable only for energies approaching several MeV, thus we will not take it into account.

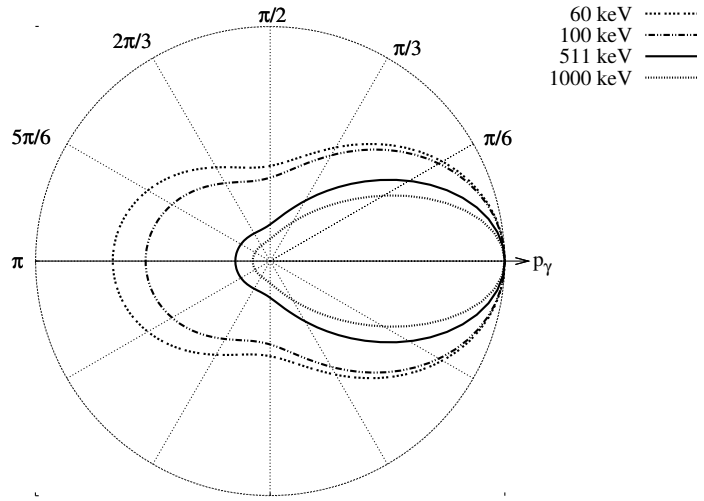

Figure 2.1: Polar plot of the Klein-Nishina formula for different incident energies.The radius of the plot represents the probability for the photon to be scattered in each angle.

2.1.1 Backscattering

A model allowing the calculation of the number of photons backscattered by the soil is necessary. In order to obtain an analytical approximation of the number of photons scattered in each volume element of the soil, let us suppose the simplified setup shown in Figure 2.2 [2].

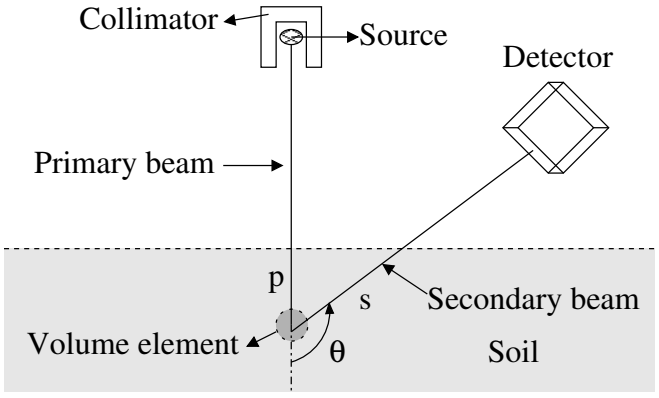

Figure 2.2: Simplified set-up to model the backscattering of radiation in soil.

A collimated and monoenergetic source is placed above the soil. It is assumed that there will be no interactions of radiation in the air between the source and the soil. The number

of photons reaching the detector per unit time, scattered in the volume element dV, dS, is given by

$$dS = N_0 \exp\left(\int \mu dl_p\right) \frac{d\sigma}{d\Omega} \Delta\Omega \rho_e dV \exp\left(-\int \mu' dl_s\right) + M(dV; s, p). \tag{2.3}$$

After reaching the soil, the primary beam travels a distance p before interacting in the volume element dV. The number of photons reaching this volume element per unit time is given by the number of photons emitted by the source per unit time, N_0, multiplied by the exponential attenuation of the beam. The scattering probability is given by the Klein-Nishina formula multiplied by the solid angle subtended by the detector from dV, $\Delta\Omega$, and by the number of electrons in the volume element. After being scattered, the secondary beam travels a distance s through the soil, in the direction of the detector. In this path, the beam is also attenuated. By assuming a detector with 100% efficiency, all the photons which go out of the soil will be recorded. We have added a multiple scattering contribution, $M(dV; s, p)$, to take into account all the photons that interact several times in the soil and finally go out in the direction of the detector. This multiple scattering contribution has no analytical expression and must be determined by simulation or by direct measurements. We can see that this simple model suggests that the number of backscattered photons depends on the electronic density of the medium and therefore this method may be suitable for detecting electronic density differences in the soil. As the multiple scattering contribution for a given volume element gives us no information about the electronic density of that particular volume element, it is considered as background and should be subtracted from the detected signal. It is possible to use it in order to analyze the backscattering of radiation in the soil [1].

2.2 Radiation detectors characteristics

This section describes the main characteristics of the detectors used and the electronics associated. The operation principle of all detectors is the same, in general the radiation leaves all or part of its energy in the mass of the detector where it is transformed in another form, a charge or voltage signal. For charged particles, the interaction with the detector volume consists of ionization of atoms of the material. Neutral particles as neutrons or γ-rays, must first undergo some kind of reaction inside the detector in order to create charged particles to ionize the atoms. The particular way of collecting this ionized charge depends on the material of the detector and in its design. In spite of the many types of detectors, some general properties may be defined for all of them. The most important are:

- Sensitivity: defined as the capability of a particular detector to produce a useful output signal for a given type of radiation as a function of energy.

- Detector response: it refers to the characteristics of the output signal produced by the detector. This implies that the response of the detector determines whether or not it is suitable for spectroscopy or if it is useful only in counting events.

- Energy resolution: it referes to the capability of distinguishing two energies lying close to each other. An ideal detector will show a sharp delta function for each detected energy, nevertheless, real detectors show a Gaussian shape characterized by its Full Width at Half Maximum (FWHM). This width arises because the uncertainty in the number of ionizations produced inside the detector volume, because of electronic noise inside it or in the electronic modules following the detector or because incomplete charge collection. The resolution of a detector at the energy E_γ is defined as

$$\text{Resolution} = \frac{\text{FWHM}}{E_\gamma}$$

  and it is usually expressed as a percentage.

- Response time: it is the time that the detector takes to form the signal after the arrival of the radiation. For a good timing, the signal should have two characteristics: first, its leading edge should be as close as possible to a vertical line. In this way a precise moment is marked by the signal as the beginning of the event; second, the duration of the signal should be as short as possible.

- Detector efficiency: efficiency refers to the amount of the incident radiation that the detector converts to a measurable pulse. Two types of efficiency are defined, the absolute efficiency and the intrinsic efficiency. The absolute or total efficiency is defined as the ratio between the number of events recorded by the detector and the number of events the source actually emitted. The intrinsic efficiency is defined as the ratio between the events registered by the detector and the fraction of photons emitted by the source that reach the volume of the detector.

- Dead time: it is the time the detection system needs to process a signal arriving to the detector, and is closely dependent on the response time. It is the result of the time the detector needs to produce a signal and the time the electronic modules following the detector require to process the pulse. Dead time does not only depend on the response time of the detector, but also on the rate of events arriving to it.

2.2.1 Scintillation detectors

Scintillators are materials (solid, liquids or gases) that produce sparks or scintillations of light when radiation passes through them. Three main groups are defined: organic crystals, inorganic crystals and gaseous detectors. The response of a scintillator to γ radiation is linear, thus the energy of the light produced by the scintillation will be proportional to the energy deposited by the radiation in the detector volume. The amount of light produced by a scintillator is very small and needs to be amplified before recording it as a pulse, the device in charge of this light amplification is known as a photomultiplier tube (PMT). This is an evacuated tube with a photocathode at its entrance and dynodes inside it. The photons coming from the scintillator collide with the photocathode, usually made of caesium or antimony, and electrons are emitted. The charge produced in the photocathode is proportional to the energy of the light colliding with it, thus the total amount of charge produced is proportional to the energy of the incident radiation. Electrons created in the photocathode are guided by an electric field successively to the dynodes, which are covered with a substance that emits secondary electrons. At the end of this amplification process, the PMT delivers an output charge pulse around 106 times stronger than the original. After amplification, charge goes to a sequence of electronic modules in order to be recorded. Due to thermionic emissions from the photocathode, PMT will always have an intrinsic noise called dark current. This effect will contribute to the dead time of scintillators.

Organic Scintillators

Organic scintillators are materials classified as aromatic compounds and consists of planar molecules of carbon chains. The detector itself is obtained by combining appropriate organic compounds in different concentrations. The substance with the highest concentration is called solvent, and the other substances are called solutes. For this kind of detectors the light emission is a result of molecular transitions: ionizing radiation passing through the detector may give some part of its energy to a molecule and rise it to an excited state. In order to decay to the ground state the molecule undergoes two processes. In first place, it releases some of the energy through lattice vibrations, a process that dissipates the energy as heat. After that, the molecule emits a photon to reach the ground level. Since part of the incident energy was previously dissipated, the photon is emitted with lower energy, as a visible light photon. For organic scintillators, the time needed to form a signal is of some nanoseconds, thus this kind of detectors are very useful for timing applications.

2.2.2 Semiconductor detectors

Germanium and silicon detectors are the most common materials used to build semiconductor or solid state detectors. The mechanism of charge collection in solid state detectors is based on the creation of electron-hole pairs inside the crystal structure: in semiconductors, the valence band and the conduction band are separated by a small energy gap of around 1 eV. If temperature is low enough to avoid electrons to go to the conduction band because of thermal fluctuations, γ radiation interacting with the detector volume will create electron-hole pairs, that we can subsequently collect using an electric field. As the energy gap for germanium is of only 0.67 eV, a temperature as low as 77 K is needed to avoid thermal effects. The gap for silicon is of 1.12 eV, thus these detectors may be operated at room temperature. In semiconductor detectors, the amount of charge produced is also proportional to the energy of the incident γ-ray. Energy resolution depends on the precise collection of the charge created by radiation, and this in turn depends on the number of electron-hole pairs produced and on the mobility of these charge carriers inside the crystal. It is important to realize that every semiconductor crystal has some impurities (that can render the crystal p-type or n-type), and large impurities concentrations may affect the mobility of the charge carriers. Nowadays, the most common semiconductor detector for γ radiation is the high purity germanium detector (HPGe or Ge) which can be produced in many shapes, as planar, coaxial or well type, in order to fulfill the experimental requirements. The timing characteristics of semiconductors are determined by the charge collection mechanism. As charge carriers must travel to the corresponding electrode, the time needed to completely collect the charge produced by a γ-ray depends on the position in the crystal where the photon interacted, thus, each output pulse has a different form. A typical time for signals in a Ge detector to be collected is about 120 ns, making this detector a very slow one.
Semiconductor detectors have a high energy resolution, but their efficiency is very low and its response time is very long. For scintillators, the response time can be as short as some nanoseconds (for some plastic scintillators), but they have a poor energy resolution. The election of detectors to be used depends on the particular goals of the experiment and on the availability of equipment. The present work used a Germanium detector to obtain precise information about the energy of the γ-rays and a plastic scintillator to have a precise timing information.

2.3 Soil physical properties

Soil is a heterogeneous porous system composed by three natural phases: the solid phase or the soil matrix (formed by mineral particles and solid organic materials); the liquid phase, which is often represented by water and which could more properly be called the

soil solution; and the gaseous phase, which contains air and other gases. This three-phase system is characterized by physical properties, some of which are described below.

2.3.1 Soil density

As part of the total volume occupied by soil may be water or air, it is useful to define two different densities to characterize a soil sample [12]. In first place we have the bulk or dry density, defined as the mass of the solid phase divided by the total volume of the sample. It is

$$\rho_{\text{bulk}} = \frac{M_s}{V_t} = \frac{M_s}{V_s + V_l + V_g}, \tag{2.4}$$

where M_s is the mass of the solid phase, V_t is the total volume of the sample and V_s, V_l and V_g represent the volume of solids, liquids and gases respectively. To take into account the liquid phase present in soil, a wet density is defined as

$$\rho_{\text{wet}} = \frac{M_t}{V_t} = \frac{M_s + M_l}{V_s + V_l + V_g}, \tag{2.5}$$

where M_t is the total mass of the sample and M_l is the mass of the liquid phase. Here we assume that the mass of air is negligible.
The wet density of a sample of soil is obtained by measuring or calculating the total mass of the sample and its total volume. The accuracy of the result depends on the methods used to measure the mass and the volume. To obtain the bulk density, the sample is placed in an oven at 105℃ for approximately 24 hours to evaporate the liquid phase and obtain the mass of the solid phase.

2.3.2 Soil water content

Several fields of science require knowledge of the amount of water contained in a particular soil volume. This is called the water content. It may be defined in two different ways: Gravimetric or volumetric. The gravimetric water content is expressed as a relation between the mass of the liquid phase and the dry mass of the soil as

$$\theta_m = \frac{M_l}{M_s} \tag{2.6}$$

The volumetric water content is given by the relation between the volume occupied by the liquid phase and the total volume of the sample. It is

$$\theta_v = \frac{V_l}{V_t} = \theta_m \frac{\rho_{\text{bulk}}}{\rho_{\text{water}}} \tag{2.7}$$

where ρ_{water} is the density of the water. The conversion between gravimetric and volumetric water contents requires knowledge of the bulk density of the soil. The standard method to determine the gravimetric water content of a sample is thermogravimetry. This is a direct method, in which a soil sub-sample is weighed before and after being dried in an oven. The conventional protocol is to warm the samples at 105 ℃ until the soil mass becomes stable. This process usually requires 24 to 48 hours, depending on the sample size and soil characteristics. The differences between the mass of the wet and the dry sample is the mass of water in the original sample. Although there are other methods to measure the water content of soil, as the neutron scattering and electric resistance methods, thermogravimetry is the one used to calibrate the indirect techniques.

CHAPTER 3

EXPERIMENTAL SETUP

The following sections describes the geometrical and electronic setup used in all experiments. It was studied the interaction of γ radiation with soil, using the backscattering of 511 keV γ-rays through farming soil. Also, a discussion about the preparation of the soil samples is made.

3.1 Geometrical Setup

The schematic arrangement of the experimental setup used for the backscattering experiments is shown in Figure 3.1. A sample of soil of variable thickness $0 < z < 18$ cm is arranged within a cubic acrylic container of base area 20×35 cm^2. It was important that the container was built with materials of low atomic number, to keep the background coming from the interaction of radiation with the box walls as low as possible. A ^{22}Na γ-source is sticked at the geometrical center of the container base. At the same side of the soil sample, at about 20 cm a plastic detector, and as close as possible to the container a germanium detector, are placed. Radioactive source and plastic detector are separated from the Ge detector by a 5 cm thick lead wall in order to avoid direct radiation source-Ge or scattering events plastic-Ge. The entire array is placed atop a γ-absorbing lead base that serves the goal of hindering Compton scattering not originating in the sample.
The source used was an IDB Holland standard sealed ^{22}Na source, model CAL2600 with an activity of 1 MBq in July 2007. ^{22}Na decays by β^+ emission to an excited state of ^{22}Ne and then a 1274.5 keV γ-ray is emitted, as shown in the decay scheme of Figure 3.2. When interacting with an electron of the medium, the positron annihilates and produces two γ-rays of 511 keV traveling in opposite directions. In this arrangement, if one of the

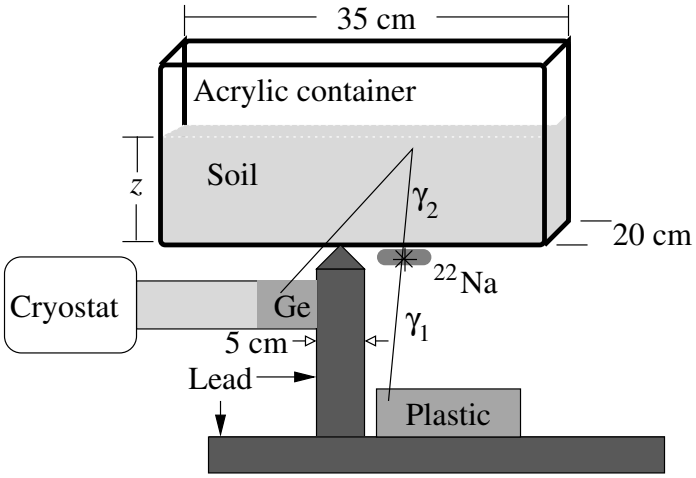

Figure 3.1: Schematics of the experimental setup used for the backscattering experiments.

511 keV γ-rays of the ^{22}Na positronic decay, e.g. γ_1, is emitted in direction to the plastic detector, the other one, γ_2, may interact with the soil and perform backscattering (SS or MS) towards the Ge detector. In this event fast electronic coincidences plastic-Ge will read the energy of the γ-ray detected in the Ge.

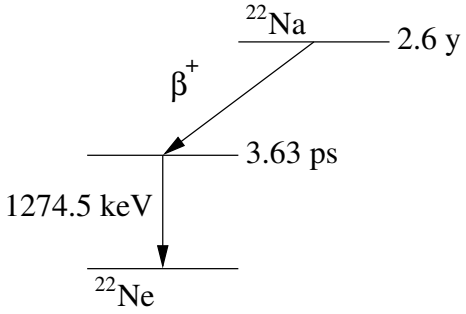

Figure 3.2: Decay scheme of ^{22}Na.

The plastic scintillator is a Scionix Holland detector, coupled to an Ortec photomultiplier base, with preamp and power supply; the size of this detector are 5 cm in diameter and 5 cm in length. The Ge detector is a Canberra GC1019 coaxial germanium detector, of 4.65 cm of diameter and 4.75 cm of length attached to a canberra Big Mac cryostat.
By connecting the Ge and the plastic scintillator in coincidences, the energy spectra recorded by the Ge allows us to study the backscattering of radiation in soil. Layers of soil from 1 cm up to 17 cm, were placed in the container and the backscattering spectra was recorded in the Ge for 30 minutes for each soil layer because the lower counting

statistics. The experiment was repeated varying soil water content. It is to note that for backscattering the 1274.5 keV γ-ray coming from the ^{22}Na source will contribute to accidental coincidences and thus will represent a background for all measurements. Although connecting the detectors in time coincidences reduces this contribution, it will always be present in the measurements.

3.2 Electronic Setup

Once the charge produced by the radiation inside the detector is collected, it is necessary to convert it into a signal that can be processed by humans in order to extract the information carried by each pulse. This process is done by a sequence of electronic modules that can be analog or digital. The first achievement of this work was to properly setup, it was previously configured [1], and make a fine tuning of the electronic setup known as time coincidences using the fast electronic modules available. Figure 3.3 shows the block diagram of the fast coincidences electronic configuration.

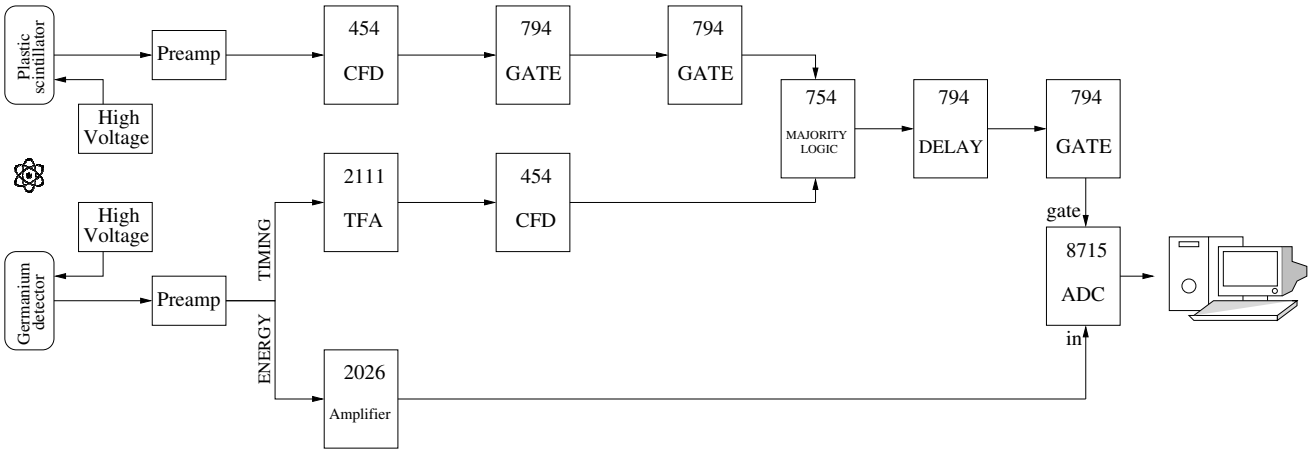

Figure 3.3: Block diagram of the electronic configuration of fast coincidences.

Each detector is connected to a voltage source. The voltage pulse comming from the preamplifier of the plastic scintillator is fed to a Constant Fraction Discriminator (CFD) to obtain a square pulse. This pulse passes through a two-stages gating process before being fed to the logic unit. The output pulse of the Ge detector goes to two different electronic branches. In one hand, it is fed to a Timing Filter Amplifier (TFA) to obtain a narrower pulse. After that it goes to a CFD and to the logic unit. The output of the logic unit is a square pulse indicating weather or not the pulses from both detectors arrived in coincidences. On the other hand, the signal is fed to an spectroscopic amplifier in order

to measure its energy. An Analoge-to-Digital Converter (ADC) is in charge of processing the energy pulses arriving in coincidences in both detectors.
We explain the electronic setup by division of this in three electronic lines: (i) "plastic line", (ii) "Ge time line" and (iii) "coincidence line".

Plastic line

Figure 3.4 shows the part of the electronic configuration is considered in the *plastic line* and also the pulses obtained as output of electronic modules. Each one of the detectors needed high voltage to operated, for the case of the plastic scintillator it is of 1000 V. The charge pulse must be converted in a voltage pulse, this is done in a module called preamplifier. The rise time of this voltage signal depends on the charge collection mechanism, for the case of the plastic scintillator, the rise time depends on the decay time of the excited states of the crystal molecules, and for the detector used it was around 7 ns. This is a very fast detector, although its energy resolution is so poor that it is not possible to distinguish a photopeak. It is to note that the pulses coming from the plastic detector have a uniform rise time. Figure 3.4 a) shows the output pulse of the plastic detector preamplifier. Because of the difference in the timing characteristic of the two detectors used, the signals coming from them need a different electronic processing. For the case of the plastic scintillator, the preamp output pulse is good enough to be used to determine a time of occurrence of the event.

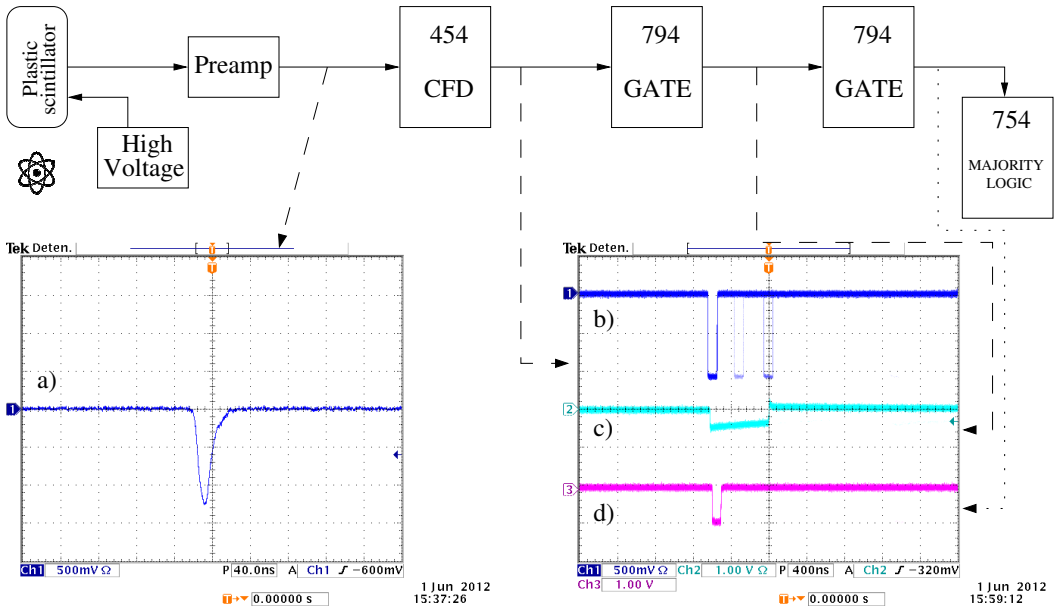

Figure 3.4: Block diagram and output pulses of the electronic modules in the plastic line.

This was done by feeding this signal into a Canberra Quad Constant Fraction Discriminator Model 454. The delay time selected for this detector was of 5.4 ns. For the case of the module used, this time is selected by varying the length of a lemo cable connected to the front of the module. The output pulses of the CFD are shown in Figure 3.4 b). We can see from the Figure that these output pulses are emitted at many different times and create what is called time jitter. This effect is generated because of the noise in the detector. The CFD has a threshold than can be modified to avoid the module to process low amplitude signals, than can be considered as noise, nevertheless because of the detector low resolution, all the signals produced by the plastic scintillator have low amplitude, then it is not possible to eliminate the noise in this way. Then, to overcome this jitter, the logic output pulse of the CFD goes to a Phillips quad gate/delay generator Model 794, where the width of the signal c) in the Figure 3.4 is set to be long enough to envelop all the jitter. Although the latter signal can be used to mark the time of arrival of the γ-ray to the plastic scintillator, it is too wide to be used as an input for the next electronic stages, thus it is processed again by the gate/delay generator and converted in a 100 ns wide logic pulse, this is show in the Figure 3.4 d).

Ge timing line

Figure 3.5 shows the part of the electronic configuration is considered in the *Ge time line* and also the pulses obtained as output of electronic modules. The operation voltage of the Ge detector is 3500 V. The charge pulse must be converted in a voltage pulse with the preamplifier. The rise time of the voltage signal depends on the charge collection mechanism, for the case of the Ge it depends on the specific place inside the crystal where each photon interacts, on the size of the crystal and on the intensity of the electric field inside it; the Ge detector is a slow detector, which in turn means it has a high energy resolution, and rise times of signals coming from it may last as long as some μs. The pulses coming from the germanium have different rise times because of the dependence with the interaction position. Figure 3.5 a) shows a typical output pulse from the Ge preamplifier. The output labelled as "Timing" has an impedance of 50 Ω and is used to obtain the information about the time of occurrence of the event. Since this signal is too wide, it cannot be used as an input to the CFD, then it is fed into a Canberra Timing Filter Amplifier Model 2111 in order to make it narrower. Figure 3.5 b) shows the output signal of the TFA. This new signal is fed into the Canberra CFD to obtain a logic pulse indicating the moment of occurrence of the interaction. For this case the delay chosen was 50 ns. Figure 3.5 c) shows the logic pulse generated in the CFD by the pulse coming from the TFA. We can see that for the Ge, the output of the CFD does not present the same jitter than for the plastic detector. This is because in this case, it is possible to set the threshold level to avoid the noise. The output of the CFD, requires no further

processing and can be used as a time stamp for the germanium detector.

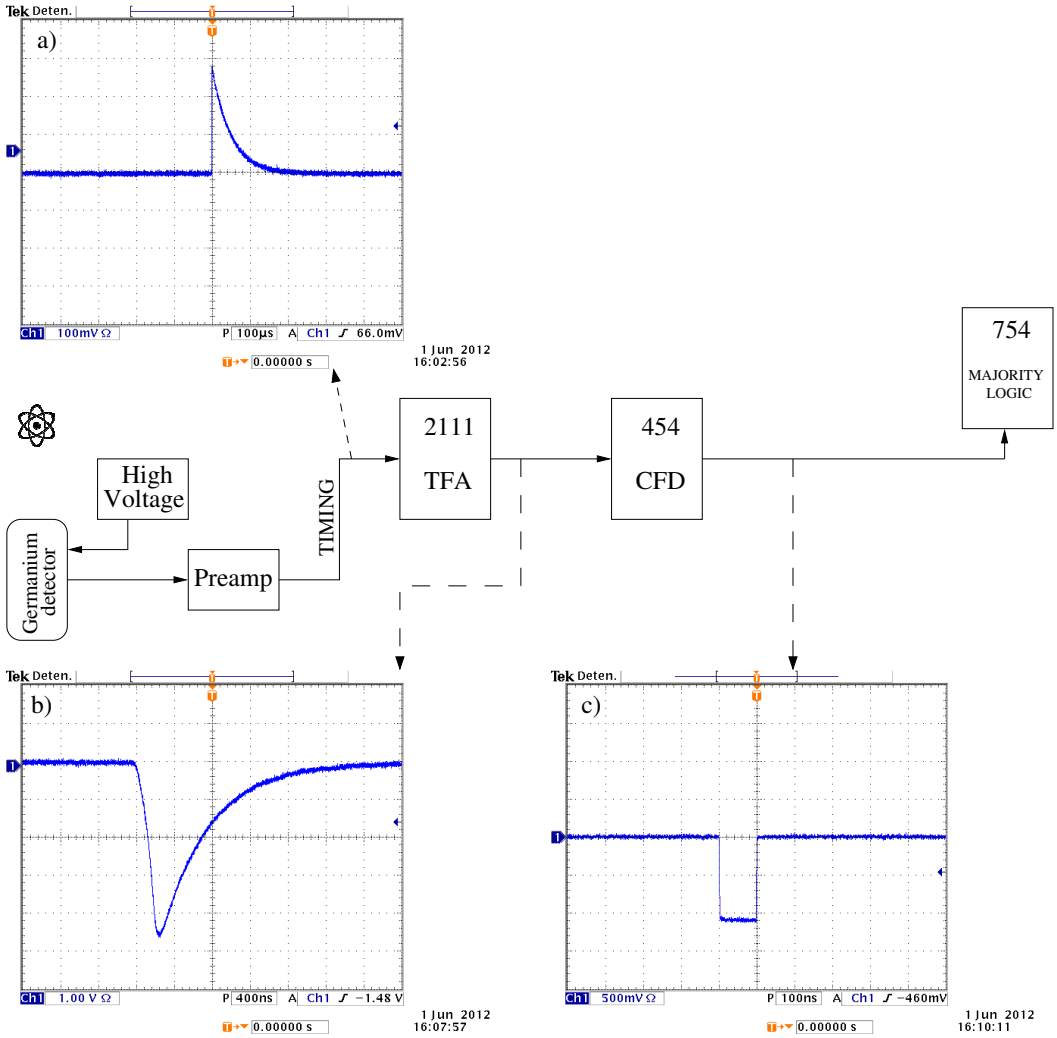

Figure 3.5: Block diagram and output pulses of the electronic modules in the Ge timing line.

Coincidence line

The next electronic stage is to compare the arrival time of the photon to each detector to determine if they arrive within certain period or time. This operation was done in the Phillips Quad Majority Logic Model 754 module. The logic pulses obtained both from plastic scintillator and from Ge are used as inputs of the majority logic module, to obtain a logic pulse indicating a coincident events.

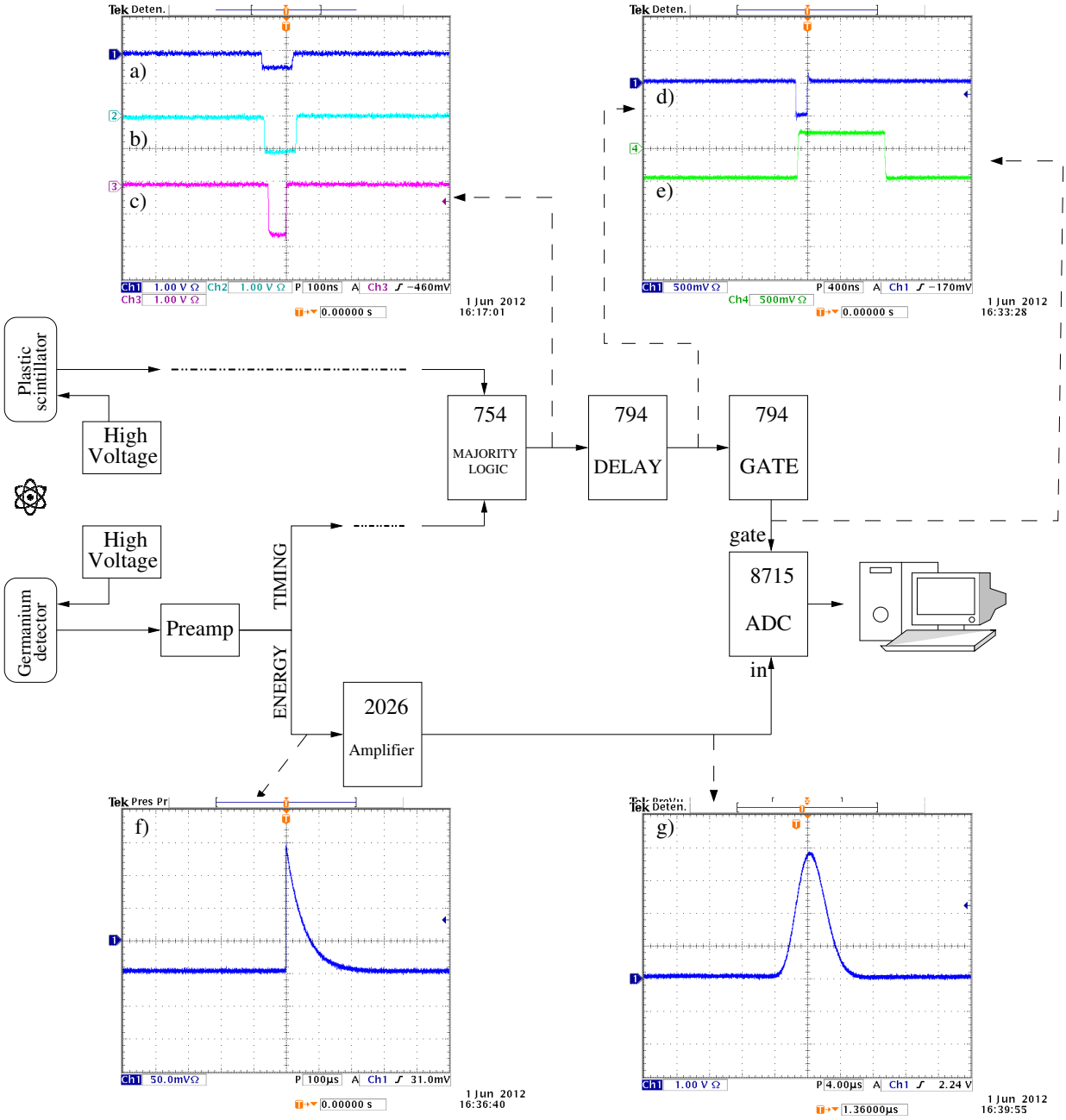

Figure 3.6: Block diagram and output pulses of the electronic modules in the coincidence line.

Figure 3.6 shows the part of the electronic configuration is considered in the *coincidence*

line. The time stamps of each detector, Figure 3.6 a) for the Ge and Figure 3.6 b) for the Plastic, which are fed into the majority logic as well as the output pulse of this latter module. The output pulse from the majority logic module is show in the Figure 3.6 c) and needs to be processed by a gate/delay generator in order give it some delay before using it in the next and last stage of the electronic setup, Figure 3.6 d) and e) show the resulting square pulse after the delay and gate processes respectively. The second output signal of the Ge detector is labeled as "Energy" and has an impedance of 93 Ω. This signal is used to obtain information about the energy deposited by radiation in the volume of the detector. This is done by feeding this signal into a Canberra Spectroscopy Amplifier Model 2026, which gives a semi-Gaussian shape to the pulse with an amplitude proportional to the energy of the incident radiation. Figure 3.6 f) shows the original pulse coming from the preamplifier and Figure 3.6 e) shows the semi-Gaussian signal obtained from the amplifier.

3.3 Samples Preparation

The experiment was performed with farming soil, found at the campus of the Universidad Nacional de Colombia. It was dried for 24 hours, then it was reduced to powder in order to remove the aggregates and finally it was sieved with a 1 mm sieve in order to guarantee its homogeneity. In this case, experiments were performed varying the water content from 0% to 25% and measurements were repeated several times because of the experimental difficulties as keeping the soil density constant, and the fact that this soil type absorbed water from the air, making difficult the water content measurement. In order to obtain the exact composition of each type of soil, X-ray fluorescence (XRF) measurements were performed at the XRF Laboratory of the Universidad Nacional de Colombia. Table 3.1 indicates the composition of the farming soil used in the experiment [1].

In order to ensure homogeneity in the samples, the humidification process was performed in a very careful way: a small amount of dry soil, approximately 300 g was mixed with the amount of water needed to obtain a given water content. The mixing process was repeated until all the dry soil was mixed with water and then all the wet soil was placed together and mixed again. Once the soil was uniformly wet, layers of different thickness of this soil were placed inside the plastic container and a measurement was made. It was important to keep the container of the wet soil covered in order to minimize the amount of water being evaporated. Also, a more accurate measurement of the water content was made by thermogravimetry. After the measurements corresponding to each water content percentage were finished, the soil was dried again in an oven for 24 hours and the process was repeated for the next water content wanted. For the experiments it was of prime importance to keep the wet density constant for the different thicknesses of the soil for a

Element or Compound	Concentration	Element or Compound	Concentration
SiO_2	60.57%	Al_2O_3	12.89%
Fe_2O_3	2.40%	CaO	1.54%
MgO	0.69%	TiO_2	0.57%
P_2O_5	0.51%	K_2O	0.49%
Na_2O	0.55%	MnO	0.04%
Ba	476 ppm	S	244 ppm
Zr	191 ppm	Sr	162 ppm
V	118 ppm	Zn	116 ppm
Cr	86 ppm	Pb	44 ppm
Cu	31 ppm	Rb	23 ppm
Ni	20 ppm		

Table 3.1: Farming soil composition obtained by XRF. The components do not sum 100% as some organic matter and the heavy elements concentration cannot be determined with XRF.

given water content. To do this, the mass of soil required to fill the respective layer was fixed and carefully measured.
The data files generated in the experiments were analyzed using `c` and `c++` routine programs.

CHAPTER 4

RESULTS

Using the experimental setup, explained in the previous chapter, spectra of backscattering of 511 keV γ-rays were obtained. The next section describes the spectroscopic analysis made for different samples of farming soil with different thicknesses and water content.

4.1 Spectroscopic analysis

In order to analyze the spectra we divide the energy in three regions and study how the number of counts in each region changes when soil thickness and water content are modified. The geometrical setup of the Ge and plastic detectors together with the electronic coincidences reduces sharply the angular range within which a single-scattered γ-ray, e.g. γ_2 in Figure 4.1, can reach the Ge detector, because of the extended size of both detectors, this range can be as large as $112^\circ \lesssim \theta \lesssim 154^\circ$, which corresponds in energies to the range between, according to equation (2.1), 176.3 keV at 154° and 215.2 keV at 112°. This is the range marked by gray vertical bars in Figure 4.2 wich shows backscattering spectra for samples of dry farming soil ($\theta_m = 0.1(1)\%$) and correspondingly labeled. γ-rays detected with an energy $E_\gamma < 176.3$ keV must have scattered more than once (Multiple Scattering). The presence of counts at energies $E_\gamma \gtrapprox 215.2$ keV can be accounted for transmission of 1274 keV γ-rays from the ^{22}Ne γ-decay after the ^{22}Na positronic decay that succeed in passing through the lead shield, and reach the detector without having any interaction with soil. The contribution of photons scattered in the soil is higher that this transmission effect. We define three different energy regions: from 0 to 176.3 keV keV we have the multiple scattering region (MS), from 176.3 keV keV to 215.2 keV we have the single backscattering region (SS) and beyond this energy we have the transmission region. This

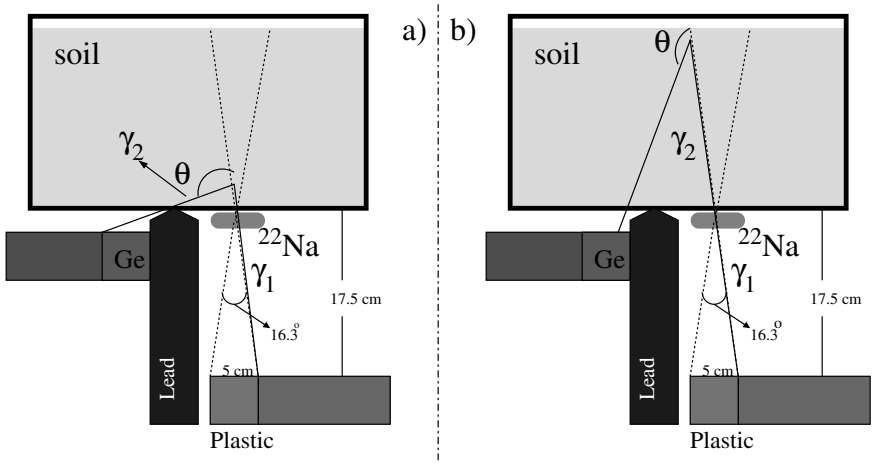

Figure 4.1: Angular range within which a single-scattered γ-ray can reach the Ge detector can be as large as $112^\circ \lesssim \theta \lesssim 154^\circ$.

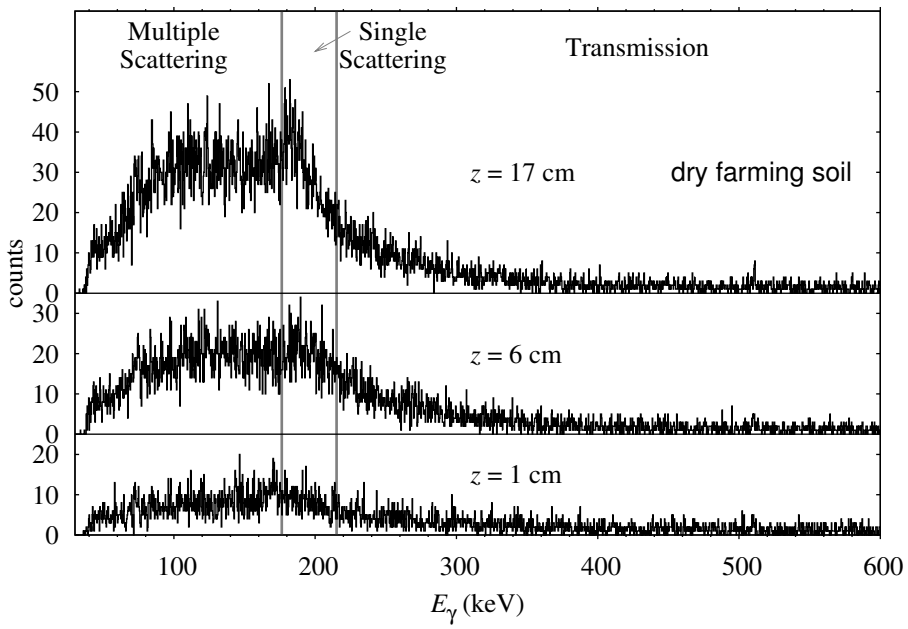

Figure 4.2: Backscattered spectra obtained for samples of dry farming soil. The three different energy regions are marked by the gray vertical lines.

division of the energy scale in three regions is totally schematic since photons of a given energy can be originated by physical processes that are here used to explain the other

regions, for example a 2-step Compton scattering may produce photons of any value in the 170−320 keV range. For the total number of counts in the spectra, counts were added up to 1300.0 keV.
Figure 4.3 shows the backscattering spectra for samples with $\theta_m = 5.6(1)\%$ and 0.96(9) g/cm^3 density. As a schema of analysis we study the number of counts in each region as a function of thickness z. Figure 4.4 shows the results for this sample.

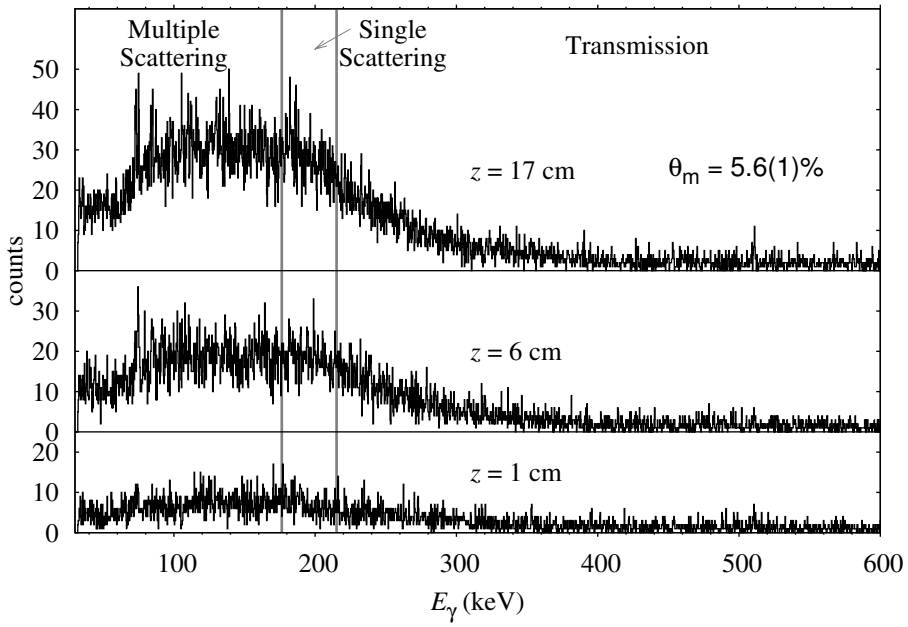

Figure 4.3: Backscattered spectra obtained for samples with water content $\theta_m = 5.6(1)\%$.

The number of counts are normalized at maximum value of total counts. We see that the total number of counts increases as soil thickness increases. For the first soil layers the increment is high, after some point the number of counts in the region seems to be constant. Table 4.1 summarizes the backscattering intensity in each espectroscopy region depicted in Figure 4.3 for this sample. We expected that the number of counts in the transmission region to be constant, i.e. independent of the soil thickness. A possible explanation on the dependence observed in the spectra is that because of the absence of collimation on the source some of the photons that are emitted can reach the soil, be scattered in angles lower than $\pi/2$ and reach the Ge detector while the time window is open. Also be considered the 1274 keV γ-rays that may interact with the soil and perform backscattering simple or multiple. The effect is visible for this experiment and could be minimized by reducing the time window.

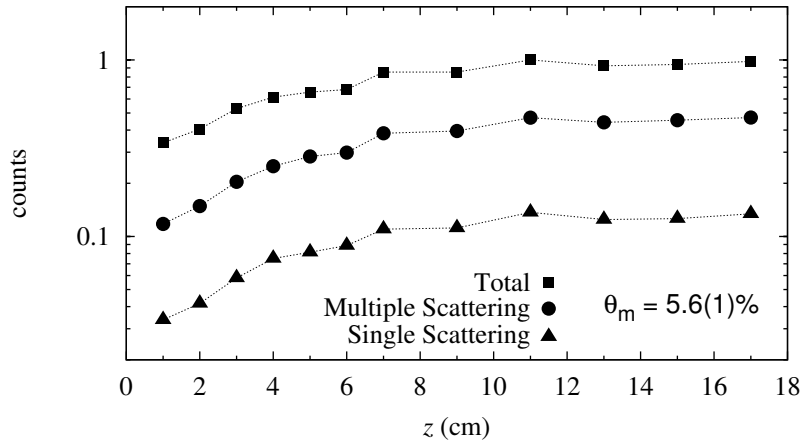

Figure 4.4: Number of counts in the energy regions as a function of layer thickness for $\theta_m = 5.6(1)\%$.

Table 4.1: Backscattering intensity in each espectroscopy region depicted in Figure 4.3.

$\theta_m = 5.6(1)\%$ $\rho_{\text{wet}} = 0.96(9)\text{g/cm}^3$	Total Scattering	(MS) Multiple Scattering	(SS) Single	Transmission	SS/MS
$z \pm 0.3$ (cm)	counts (10^4)				
1	0.81	0.28	0.08	0.45	0.29
2	0.97	0.36	0.10	0.52	0.28
3	1.27	0.49	0.14	0.64	0.29
4	1.47	0.60	0.18	0.69	0.30
5	1.58	0.68	0.19	0.70	0.29
6	1.63	0.71	0.21	0.70	0.30
7	2.05	0.92	0.26	0.86	0.29
9	2.04	0.95	0.27	0.83	0.28
11	2.40	1.13	0.33	0.94	0.29
13	2.22	1.06	0.30	0.86	0.28
15	2.26	1.09	0.30	0.86	0.28
17	2.35	1.13	0.32	0.90	0.28

The ratio SS/MS for the samples analyzed in the present work are summarized in the Table 4.2. The ratio SS/MS states that Multiple and Single scattering intensities are, for the first approximation, independent of water content and constant for each soil layer thickness.

Figure 4.5 shows the ratio SS/MS for the samples analyzed as function to thickness.

Table 4.2: Ratio SS/MS for the samples analyzed in the present work.

$\theta_m(\%)$	0.1(1)	5.6(1)	9.2(1)	12.4(1)	21.3(4)
$\rho_{\text{wet}}(\text{g/cm}^3)$	0.9(2)	0.96(9)	0.91(9)	0.87(8)	0.81(1)
$z \pm 0.3$(cm)	SS/MS				
1	0.31	0.29	0.32	0.32	0.32
2	0.30	0.28	0.29	0.28	0.31
3	0.29	0.29	0.30	0.27	0.29
4	0.32	0.30	0.28	0.29	0.30
5	0.31	0.29	0.29	0.29	0.32
6	0.33	0.30	0.28	0.27	0.32
7	0.32	0.29	0.29	0.29	0.33
9	0.32	0.28	0.28	0.29	0.33
11	0.31	0.29	0.28	0.31	0.33
13	0.32	0.28	0.27	0.28	0.32
15	0.32	0.28	0.26	0.28	0.32
17	0.30	0.28	0.28	0.27	0.31
⟨SS/MS⟩	0.31(1)	0.29(1)	0.29(1)	0.29(1)	0.32(1)

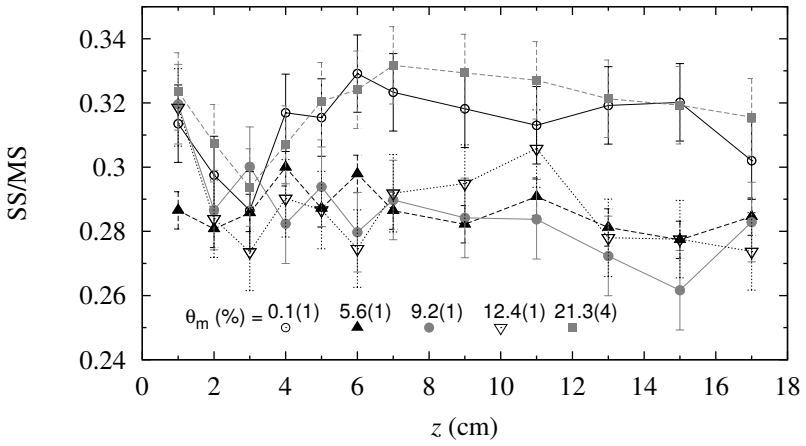

Figure 4.5: Ratio SS/MS as function to thickness for samples with different θ_m.

The last row of the Table 4.2 indicate the average value ⟨SS/MS⟩ for each water content point. The average values start at around 0.31 for the lower water content, decrease and accumulate around 0.29 for the intermediate values of θ_m and rising again to 0.32 for $\theta_m = 21.3\%$. We found that the average ratio SS/MS for the farming soil is 0.30 ± 0.01. The results are useful because we are supposing that the quality of the obtained image in

the Compton camera, explained in the Chapter 1, can be improved by taking into account only photons that undergo single scattering in the soil then, for the ratio SS/MS, we find the proportion of photons that may contribute to image formation is 30% of the photons that reach de backscattering detector.

4.2 Comparison results for sand and farming soil

As an example, Figure 4.6 compares the number of counts in each region as a function of thickness z for both dry sand and dry farming soil. Figure 4.6 shows that dry sand is a much better γ-backscatterer than dry farming soil.

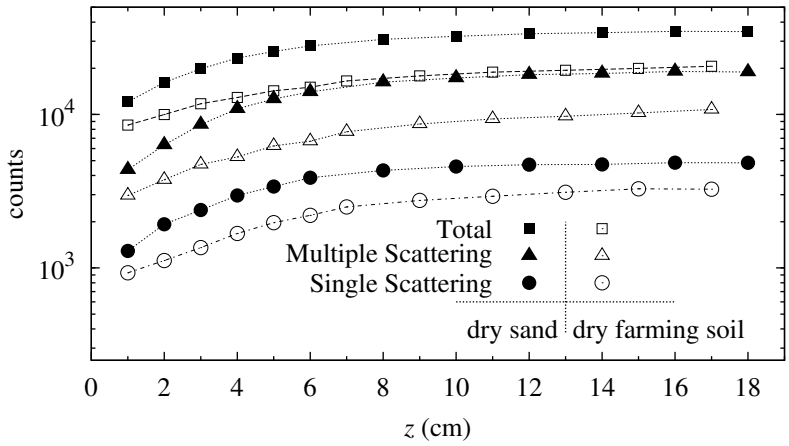

Figure 4.6: Number of counts in the energy regions as a function of layer thickness for dry sand and farming soil

Table 4.3 summarizes the backscattering intensity in each espectroscopy region for for both sand and farming soil samples with the highest thickness: 17 cm for farming soil and 18 cm for sand. This indicates that the ratio SS/MS for the dry farming soil is bigger that the same relation for dry sand. For farming soil de ratio SS/MS is 0.30 and for sand is 0.25. The results indicate that for a soil with higher density is obtained a greater proportion of multiple scattering. This result also is an important piece of information since it means that this type of measuremenrt is able to distinguish types of soil.

Table 4.3: Backscattering intensity in each spectrsocopic region for dry sand and dry farming soil.

	sand	farming soil
θ_m (%)	0.02(1)	0.1(1)
ρ_{wet} (g/cm^3)	1.58(8)	0.9(2)
	counts (10^4)	
Multiple Scattering	1.89	1.07
Single Scattering	0.48	0.32
Transmission	1.09	0.66
Total	3.46	2.06
SS/MS	0.25	0.30

The present work is first attempt to extract physical properties of soil samples using γ-spectroscopic information. The simplified energy division proposed gives already useful unformation. Analysis over more types of samples will show the real practical usefulness. The spectroscopic aproach gives also refinement possibilities.

CHAPTER 5

CONCLUSIONS

- The geometrical setup of the Ge and plastic detectors together with the electronic coincidences reduces sharply the angular range within which a single-scattered γ-ray can reach the Ge detector, this range can be as large as $112° \lesssim \theta \lesssim 154°$, which corresponds in energies to the range between, according to equation (2.1), 176.3 keV at 154° and 215.2 keV at 112°.

- The number of counts in each region of a backscattering spectra increases as a function of soil thickness. A possible explanation on the dependence observed in the trasmission region is that because of the absence of collimation on the source some of the photons that are emitted can reach the soil, be scattered in angles lower than $\pi/2$ and reach the Ge detector while the time window is open, also some of the 1274 keV γ-rays that are emitted may interact with the soil and perform backscattering simple or multiple.

- The ratio SS/MS states that Multiple and Single scattering intensities are independent of water content and constant for each soil layer thickness. We found that the average ratio SS/MS for the farming soil is 0.30 ± 0.01.

- We are supposing that the quality of the obtained image in the Compton camera can be improved by taking into account only photons that undergo single scattering in the soil then, for the ratio SS/MS, we find the proportion of photons that may contribute to image formation is 30% of the photons that reach de backscattering detector.

- That dry sand is a much better γ-backscatterer than dry farming soil. This result

also is an important piece of information since it means that this type of measuremenrt is able to distinguish types of soil.

- The present work is first attempt to extract physical properties of samples using γ-spectroscopic information. The simplified energy division proposed in Figure 4.2 gives already useful unformation. Analysis over more types of samples will show the real practical usefulness. The spectroscopic aproach gives also refinement possibilities.

BIBLIOGRAPHY

[1] Martha Liliana Cortes Sua. Energy and Time Characterization of the response of the soil to γ-rays. Master's thesis, Universidad Nacional de Colombia, 2010.

[2] G. Harding, W. Gilboy, and B. Ulmer. Photon-induced positron annihilation radiation (PIPAR) -A novel gamma-ray imaging technique for radiographically dense materials. *Nucl. Instr. and Meth. in Phys. Res.*, A398:409–422, 1997.

[3] B.L. Evans, J.B. Martin, L.W. Burggraf, and M.C. Roggemann. Nondestructive Inspection Using Compton Scatter Tomography. *IEEE Transactions on Nuclear Science*, 45(3):950 –956, 1998.

[4] Shuo-Sheng Tang and Esam M.A. Hussein. Use of isotopic gamma sources for identifying anti-personnel landmines. *Applied Radiation and Isotopes*, 61:3–10, 2004.

[5] J. Gerl. Gamma-ray imaging exploiting the Compton effect. *Nucl. Phys.*, A752:688c, 2005.

[6] E. Fajardo, M. F. Nader, F. Cristancho, and J. Gerl. The photographic capacity of a gamma Compton backscattering device. *American Institute of Physics Conference Proceedings*, 1265:449, 2010.

[7] M. L. Cortés, L. M. Melo, and F. Cristancho. Influence of humidity on the scattering of γ-rays in soil. *American Institute of Physics Conference Proceedings*, 1265:395, 2010.

[8] J. Gómez-Muñoz, M.L. Cortés, and F. Cristancho. Gamma backscattering in soil layers with different thickness and water content. *American Institute of Physics Conference Proceedings*, 1423:418, 2012.

[9] N. González, E. Fajardo, W. Blanco, and F. Cristancho. Characterizationof a γ-backscattering imaging device. *American Institute of Physics Conference Proceedings*, 1423:359, 2012.

[10] Glenn F. Knoll. *Radiation Detection and Measurement*. John Wiley & Sons Inc., 2000.

[11] William Leo. *Techniques for Nuclear and Particle Physics Experiments*. Springer-Verlag, 1994.

[12] Malcom Sumner, editor. *Handbook of soil science*. Taylor & Francis Group, 2000.